Title
Diachronous development of Great Unconformities before Neoproterozoic Snowball Earth.

Journal
Proceedings of the National Academy of Sciences, 117(19)

Authors
Flowers, Rebecca
Macdonald, Francis
Siddoway, Christine
et al.

Publication Date
2020-05-12

DOI
10.1073/pnas.1913131117

Peer reviewed

Diachronous development of Great Unconformities before Neoproterozoic Snowball Earth

Rebecca M. Flowers[a,1], Francis A. Macdonald[b], Christine S. Siddoway[c], and Rachel Havranek[a]

[a]Department of Geological Sciences, University of Colorado, Boulder, CO 80309; [b]Earth Science Department, University of California, Santa Barbara, CA 93106; and [c]Department of Geology, The Colorado College, Colorado Springs, CO 80903

Edited by Paul F. Hoffman, University of Victoria, Victoria, Canada, and approved March 6, 2020 (received for review July 30, 2019)

The Great Unconformity marks a major gap in the continental geological record, separating Precambrian basement from Phanerozoic sedimentary rocks. However, the timing, magnitude, spatial heterogeneity, and causes of the erosional event(s) and/or depositional hiatus that lead to its development are unknown. We present field relationships from the 1.07-Ga Pikes Peak batholith in Colorado that constrain the position of Cryogenian and Cambrian paleosurfaces below the Great Unconformity. Tavakaiv sandstone injectites with an age of ≥676 ± 26 Ma cut Pikes Peak granite. Injection of quartzose sediment in bulbous bodies indicates near-surface conditions during emplacement. Fractured, weathered wall rock around Tavakaiv bodies and intensely altered basement fragments within unweathered injectites imply still earlier regolith development. These observations provide evidence that the granite was exhumed and resided at the surface prior to sand injection, likely before the 717-Ma Sturtian glaciation for the climate appropriate for regolith formation over an extensive region of the paleolandscape. The 510-Ma Sawatch sandstone directly overlies Tavakaiv-injected Pikes granite and drapes over core stones in Pikes regolith, consistent with limited erosion between 717 and 510 Ma. Zircon (U-Th)/He dates for basement below the Great Unconformity are 975 to 46 Ma and are consistent with exhumation by 717 Ma. Our results provide evidence that most erosion below the Great Unconformity in Colorado occurred before the first Neoproterozoic Snowball Earth and therefore cannot be a product of glacial erosion. We propose that multiple Great Unconformities developed diachronously and represent regional tectonic features rather than a synchronous global phenomenon.

Great Unconformity | Snowball Earth | thermochronology | zircon (U-Th)/He | injectites

The Great Unconformity is an iconic geologic feature that classically marks the boundary between unfossiliferous Precambrian rocks and fossiliferous Phanerozoic strata. To Charles Darwin (1), the "sudden appearance" of complex macroscopic fossils in Cambrian strata necessitated a global stratigraphic omission to reconcile the fossil record with Darwinian gradualism. Although subsequent concepts of extinction and radiation eliminated the need of a global time gap to explain the fossil record, the notion of a Late Neoproterozoic to Cambrian global unconformity has persisted (2–5). Particularly, the Great Unconformity in North America, where the base of the Cambrian transgressive sequence commonly overlies Precambrian basement (6), has been globally correlated with Late Neoproterozoic to Cambrian unconformities on other continents (2–5). Recently, inferred erosion across these Great Unconformities has been associated with a variety of changes in the Earth System, including the Neoproterozoic Snowball Earth (2), the initiation of modern plate tectonics (3), oxygenation of the ocean and atmosphere (4), and the Cambrian Explosion (5). However, the timing, magnitude, and causes of erosion below the Great Unconformities, and whether their development was globally synchronous or diachronous, are unknown. Although much work has focused on Cambrian sedimentary records that locally rest on older strata or that unconformably overlie basement (7–9), precisely because the Great Unconformities mark a large gap in the rock record, the erosion history leading to their formation cannot be investigated directly by study of preserved units.

Past work leads to at least four general models for the timing and magnitude of pre-Great Unconformity continental erosion, which are depicted in Fig. 1. Some have proposed major erosion of the continents associated with assembly of the supercontinent Rodinia and mantle upwelling below it prior to 850 Ma (Hypothesis 1) or with the early diachronous breakup of Rodinia between 850 and 717 Ma (Hypothesis 2) (10–17). Others argue for an association with the Cryogenian Snowball Earth glaciations from 717 to 635 Ma (Hypothesis 3) (18–22). Still others suggest that the appearance of animals and modern ecosystems was the product of nutrient delivery via erosion and an increase in atmospheric oxygen at the Ediacaran–Cambrian transition at ca. 540 Ma (Hypothesis 4) related to the "transgressive buzzsaw" and subsequent burial (4, 5), later rifting of Laurentian margins (23, 24), or the Pan-African and Transantarctic orogenies and construction of the supercontinent Pannotia (25, 26).

A critical question is if the Great Unconformity represents a single, global exhumation pulse (2, 4, 5) as the models above typically assume, or if it is composite in origin (27). It is possible that there are multiple Great Unconformities, which formed over hundreds of millions of years due to diachronous regional tectonic phenomena. Multiple spatially heterogeneous exhumation events driven by several of the above mechanisms could combine to generate one amalgamated gap of lengthy duration over a broad geographic scale. Arguments that Great Unconformity erosion surface formation was a global phenomenon use geochemical proxy data or preserved sediment volumes on North America to indirectly infer erosion flux and nutrient delivery across the Great Unconformity (2, 4, 5) rather than directly analyzing the age of the erosion surfaces. However, interpretations of these geochemical records are nonunique, and the surfaces themselves are poorly dated. Deciphering the age of

Significance

Erosion below the Great Unconformity has been interpreted as a global phenomenon associated with Snowball Earth. Geological relationships and thermochronologic data provide evidence that the bulk of erosion below the Great Unconformity in Colorado occurred prior to Cryogenian glaciation. We suggest that there are multiple, regionally diachronous Great Unconformities that are tectonic in origin.

Author contributions: R.M.F. and F.A.M. designed research; R.M.F., F.A.M., C.S.S., and R.H. performed research; and R.M.F., F.A.M., and C.S.S. wrote the paper.

Competing interest statement: P.F.H. and F.A.M. are coauthors on three papers, most recently in 2017.

This article is a PNAS Direct Submission.

[1]To whom correspondence may be addressed. Email: rebecca.flowers@colorado.edu.

This article contains supporting information online at https://www.pnas.org/lookup/suppl/doi:10.1073/pnas.1913131117/-/DCSupplemental.

First published April 27, 2020.

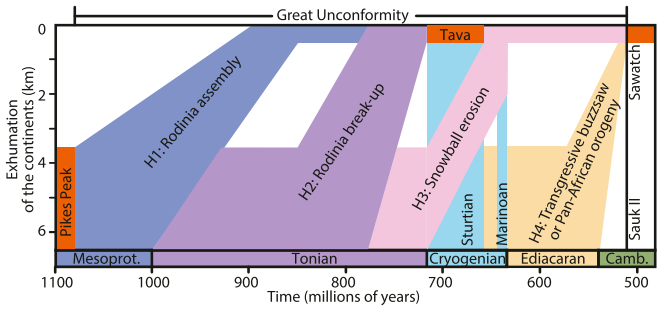

Fig. 1. Hypothesized exhumation histories below the Great Unconformity. Orange bars depict geological constraints from Colorado. Hypothesis 1 (H1) depicts major erosion of the continents associated with assembly of the supercontinent Rodinia and mantle upwelling below it (14, 17). Hypothesis 2 (H2) depicts major erosion associated with the early breakup of Rodinia (10–13, 15, 16). Hypothesis 3 (H3) depicts an association with the Cryogenian Snowball Earth glaciations (18–22). Hypothesis 4 (H4) depicts major erosion associated with the Cambrian transgressive buzzsaw and subsequent burial (4, 5), later rifting of Laurentian margins (23, 24), or the Pan-African orogeny and Transantarctic orogenies and construction of the supercontinent Pannotia (25, 26). An alternative hypothesis is that there are multiple Great Unconformities representing diachronous regional phenomena, and these features developed predominantly on Laurentia and its conjugate rifted margins.

the Great Unconformity at specific localities by constraining Precambrian basement exhumation histories prior to Paleozoic overlap assemblages is required to test the competing hypotheses for Great Unconformity formation and tease out potential complexities in its origins.

Recent work has used advances in thermochronology to constrain major cooling events preceding Great Unconformity development in the Ozark Mountains of the central United States (16) as well as the Bighorn Mountains and Wind River Range in Wyoming (28). These studies inferred major erosion associated broadly with Rodinia supercontinent breakup (16, 28). However, the Cambrian sedimentary sequences above the Great Unconformity at these localities only strictly limit development of the erosion surface to be Cambrian or older such that the thermochronologic data allow major erosion even into the latest Neoproterozoic. Consequently, these studies are unable to distinguish among the hypotheses in Fig. 1. Integration of tighter Neoproterozoic and Cambrian geologic constraints with thermochronologic data is vital to resolve cooling and erosion histories at the level required to differentiate between models for Great Unconformity development.

Here, we present an exceptional suite of Neoproterozoic and Cambrian surface constraints from the Late Mesoproterozoic Pikes Peak batholith of the southern Colorado Front Range that document that the basement was at the surface by 676 ± 26 Ma and likely before 717 Ma. These relationships provide evidence that most erosion below the Great Unconformity occurred here prior to the Cryogenian Snowball Earth glaciations, thus enabling discrimination among Great Unconformity hypotheses at this locality. Zircon (U-Th)/He (ZHe) data from samples immediately below the Great Unconformity are consistent with the geologic observations. We conclude by comparing these outcomes with those of recent work and consider the broader significance for a synchronous vs. diachronous origin of the Great Unconformities.

Geologic Setting of the Pikes Peak Batholith and Great Unconformity in Colorado

The 1.07-Ga Pikes Peak batholith is located in the southern Colorado Front Range (Fig. 2), where it intrudes ∼1.7-Ga metasedimentary rocks as well as ∼1.7- and ∼1.4-Ga rocks of the Routt and Berthoud plutonic suites (29). The batholith is dominated by the coarse-grained Pikes Peak granite (30) that was emplaced at 1,066 ± 10 Ma (31). The batholith likely crystallized at depths <5 km based on the low water content and late-stage crystallization temperatures of 720 °C to 700 °C estimated for the magmas and may even have breached the surface (32). Three areas within the batholith characterized by concentric flow structures may underpin former calderas, further supporting shallow batholith emplacement (29). At Pikes Peak, one of these intrusive centers encompasses the southern lobe of the batholith (29). Initial rapid cooling following Pikes Peak batholith emplacement is documented by 10 hornblende $^{40}Ar/^{39}Ar$ dates from 1,080 ± 3 to 1,068 ± 2 Ma, 4 biotite $^{40}Ar/^{39}Ar$ plateau dates from 1,079 ± 3 to 1,073 ± 2 Ma, and K-feldspar $^{40}Ar/^{39}Ar$ data that suggest low-temperature cooling by ∼1,000 Ma (33). An apatite

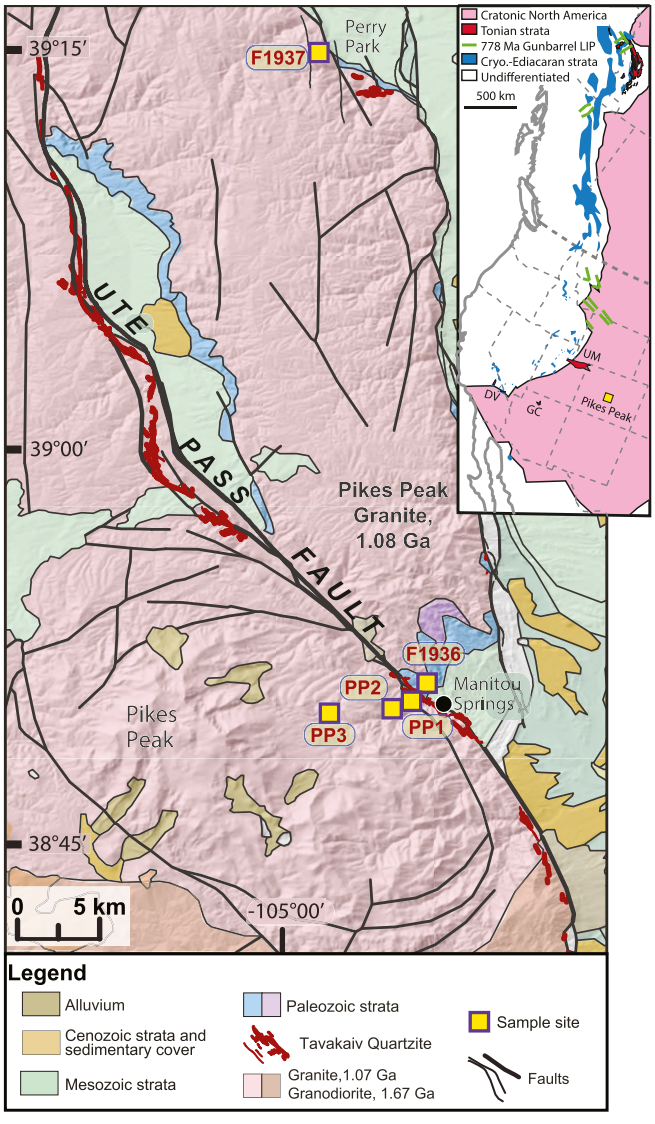

Fig. 2. Geologic map of the Pikes Peak study area with sample locations marked. The Tavakaiv injectites that indicate the position of the Neoproterozoic paleosurface are also shown. *SI Appendix*, Fig. S1 is a regional geologic map that shows the broader distribution of Tavakaiv exposures across an ∼24,000-km^2 region of the Colorado Front Range and nearby basement uplifts. *Inset* is a simplified map of the western United States that shows the location of the field area and the distribution of Neoproterozoic strata across the western United States. DV, Death Valley; GC, Grand Canyon; UM, Uinta Mountains; LIP, large igneous province.

fission track (AFT) date of 447 ± 57 Ma is available from a sample near the top of Pikes Peak and attributed to resetting during Phanerozoic burial heating (34, 35), but otherwise, the Pikes Peak granite is largely devoid of apatite and therefore, lacks AFT (34) and apatite (U-Th)/He data.

The Great Unconformity in the study area is defined where Cambrian sandstone of the Sawatch Formation nonconformably sits on Pikes Peak granite basement rock (Fig. 3*A*). Post-Sawatch strata provide a record of subsequent episodes of exposure, burial, and reexposure of the Pikes Peak batholith. In some locations, Pennsylvanian arkosic sandstone of the Fountain Formation both overlies the Pikes Peak granite (Fig. 2) and contains clasts of the granite (36, 37). Latest Cretaceous Arapahoe Formation sandstones also contain Pikes Peak granite clasts (38). Maximum preserved thicknesses of Early Paleozoic sedimentary rocks in the study region are <100 m, whereas those for the Pennsylvanian through Cretaceous section are ∼3.1 to 4 km (39–41). Together, this indicates that the Pikes Peak granite was at the surface in the Cambrian, was buried and reexposed in the Pennsylvanian, and then, was reburied and again reexposed in the latest Cretaceous.

The objective of our study is to determine when the Pikes Peak batholith was first exhumed to the surface before Cambrian sandstone deposition in order to test the hypotheses for sub-Great Unconformity erosion. As described below, Tavakaiv sandstone dikes and sills provide key constraints on the minimum timing of initial granite exposure.

Constraints on the Great Unconformity in Colorado from the Tavakaiv Injectites

The Tavakaiv sandstone is an areally extensive clastic system of centimeter- to meter-scale dikes and sills that cuts Proterozoic basement over an ∼24,000-km^2 region of the Colorado Front Range and nearby basement uplifts (*SI Appendix*, Fig. S1) (42, 43). The sandstone consists of an indurated, poorly sorted, subrounded to rounded, coarse-grained quartz sand matrix with subordinate, dispersed gravel to pebble-sized clasts of rounded quartz and angular granite and is generally maroon in color owing to presence of authigenic Fe-oxide (44). Basement-hosted sandstones are referred to as injectites because they require fluid overpressure for emplacement (42). The Tavakaiv injectites were formed by downward and lateral injection of liquified clastic sediment from a source at the surface (42). Multiple generations with clear cross-cutting relationships intruded the Pikes Peak granite along a >75-km length of the Ute Pass fault system (Fig. 2). Tavakaiv dikes and sills also cut larger Tavakaiv sandstone bodies within fault-bounded kilometer-scale "panels" between strands of the Ute Pass fault (42).

Outcrop relationships indicate that most Tavakaiv injectites were emplaced in the near subsurface (42). Some bodies have bulbous, curving margins that deform an intense fracture fabric in granite host rock, suggesting that the host rock was intensely weathered, malleable, and proximal to a free surface (Fig. 3*B*). Highly weathered, angular fragments of chloritic, oxidized granite commonly occur as clasts within strongly indurated, otherwise pristine, unweathered injectites (Fig. 3*C* and *SI Appendix*, Figs.

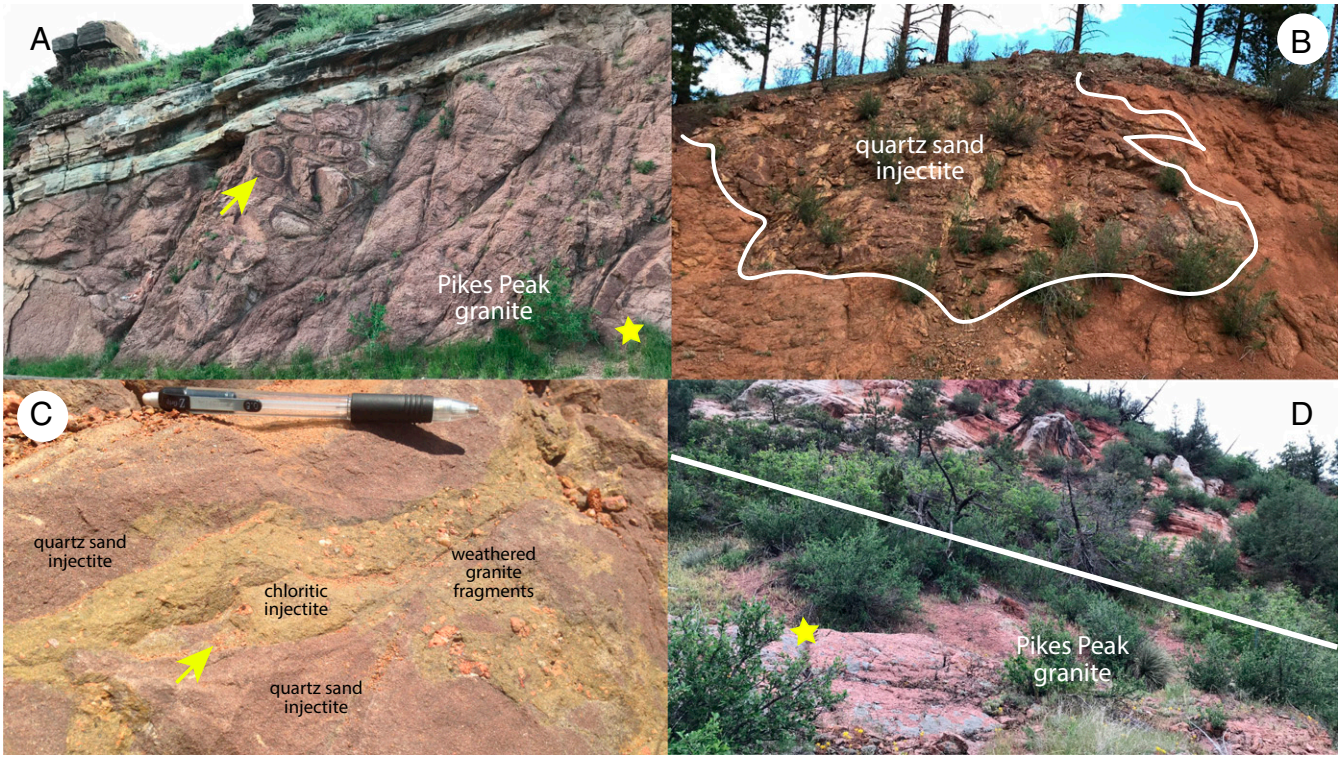

Fig. 3. Photographs illustrating key Tavakaiv injectite, Sawatch sandstone, and Great Unconformity field relationships that constrain the position of the Neoproterozoic and Cambrian paleosurfaces. (*A*) Great Unconformity near Manitou Springs, Colorado. Pikes Peak basement with ∼1.5-m-diameter core stones (marked with the yellow arrow) onlapped by sandstone of the Sawatch Formation. The yellow star is where sample F1936 was collected ∼10 m below the Great Unconformity. (*B*) Bulbous Tavakaiv injectite, outlined in white, cutting weathered Pikes Peak granite near Buffalo Creek, Colorado. (*C*) Detail of the interior to a Tavakaiv dike near Buffalo Creek, Colorado. Injected sediment consists of mature quartz sand, with red color imparted by interstitial hematite. Greenish-colored sand injectite contains abundant clasts of weathered granite, chlorite, and clays entrained from the weathered wall rock. The intermixed sediments display both sharp and gradational contacts. Image credit: Alec Lee (Colorado College, Colorado Springs, CO). *SI Appendix*, Fig. S2 shows the field context within a 7-m-wide sedimentary dike. (*D*) Great Unconformity at Perry Park with sandstone of the Sawatch Formation overlying Pikes Peak granite. The yellow star is where sample F1937 was collected ∼2 m below the Great Unconformity, which is marked by a white line.

S2 and S3 *A* and *B*) (42). The degree of weathering of the engulfed fragments and flakes of granitic wall rock indicates prolonged residence of Pikes Peak granite at the surface that caused formation of a deeply weathered granitic regolith prior to sand injection, entrainment of oxidized regolith fragments, and cementation. Some centimeter-scale Tavakaiv dikes appear controlled by brittle fracture geometries within the host granite, consistent with emplacement into fractured, weathered granite near the surface (*SI Appendix*, Fig. S3*C*). Elsewhere, there is clear evidence that some Tavakaiv dikes were injected more deeply. These dikes occur within competent granite bedrock in incised canyons >300 m below the present-day regional land surface, have long lateral continuity along faults and fractures, lack quartz pebbles and weathered basement clasts, and likely reflect emplacement depths of up to ∼1 km (42).

A Cryogenian age for the injectites is indicated by (U-Th)/He data on hydrothermal specular hematite (44). The specular hematite occurs in quartz–hematite veins inferred to have mineralized from 230 °C to 210 °C hydrothermal fluids during sand injection (44). The quartz–hematite veins cut and are cut by the Tavakaiv dikes, suggesting coeval formation (44). Thirty-one single hematite crystals of varying size isolated from polycrystalline aggregates of two specular hematite vein samples yielded (U-Th)/He dates of 717 ± 12 to 437 ± 7 Ma (44). The

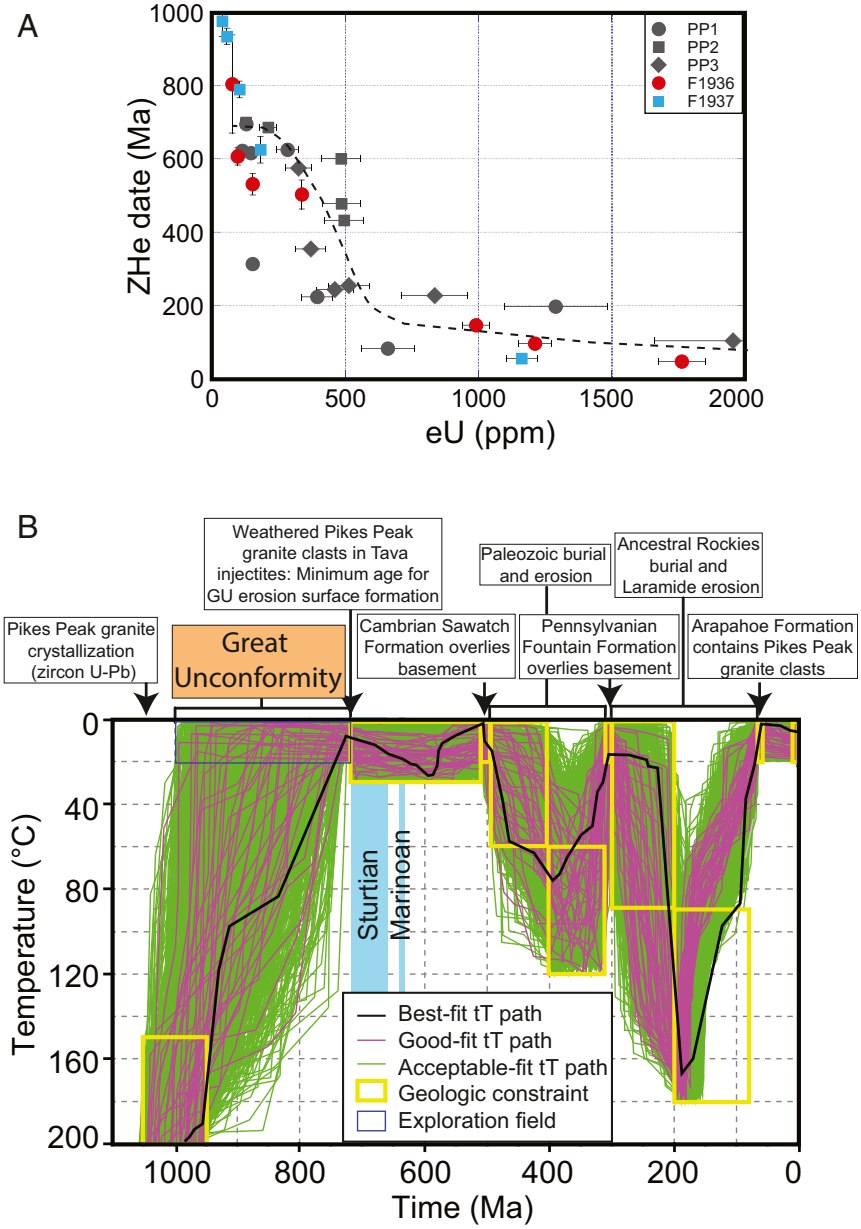

Fig. 4. ZHe data and thermal history modeling results for Pikes Peak granite samples. (*A*) Plot of ZHe date vs. eU, where the dashed curve marks the date–eU distribution predicted by the best-fit path in *B*. Uncertainties on individual ZHe dates are reported at 2σ and are based on the propagated analytical uncertainties on the U, Th, and He measurements. Uncertainties on eU values are conservatively assigned to be 15%. (*B*) Temperature–time diagram showing the inverse thermal history model result for the Pikes Peak ZHe data. This plot shows only the <200 °C temperature range, but the models begin with Pikes Peak granite emplacement at temperatures of 600 °C at 1066 ± 10 Ma followed by rapid cooling. Complete details regarding model inputs and applied geological constraints are in *SI Appendix*, Table S2. Although the best-fit path is shown to demonstrate that it reproduces the data in *A*, favoring the best-fit over the other "good-fit" paths is not statistically defensible, and we base our interpretations on the full range of good-fit results.

dates show a broad positive correlation with crystal thickness, consistent with He retentivity that varies with crystal size (44). The dates for the nine largest crystals were used to obtain a mean and uncertainty of 676 ± 26 Ma, favored as the timing of sand injection, but this date can alternatively and more conservatively be considered a minimum age for Tavakaiv emplacement (44). Thermal history modeling using hematite He diffusion kinetic data implies He loss from the hematite during subsequent burial events (44) such that the oldest suite of four hematite dates that vary from 717 to 695 Ma could represent emplacement with the remaining data array reduced to younger dates from variable He loss.

Detrital zircon U-Pb data from samples of the different Tavakaiv generations across the region are consistent with the Cryogenian injectite age. Diagnostic zircon populations are similar to those of other Neoproterozoic siliciclastic strata across the southwestern United States, suggesting approximately coeval formation from a common clastic Neoproterozoic source (43, 44). The Tavakaiv detrital zircon data are also statistically distinct from detrital zircon age distributions in Paleozoic sandstones (43, 44). In addition, a single detrital zircon from one of the Tavakaiv samples yielded a date of ∼760 Ma. Although this result is insufficient to impose a firm maximum emplacement age without being reproduced (44), it is compatible with the Cryogenian hematite (U-Th)/He age for Tavakaiv injection.

The Cryogenian Tavakaiv age and the geologic relationships documenting shallow injectite emplacement require that the 1.07-Ga Pikes Peak basement underlying the Great Unconformity was exhumed from <5-km depth (29, 32) to the surface by Cryogenian time. The ∼24,000-km^2 distribution of identified injectites marks the position of a regional Cryogenian surface that encompassed a broad swath of the paleolandscape (*SI Appendix*, Fig. S1). The injectites temporally overlap with the 717- to 660-Ma Sturtian glaciation (15, 45, 46), which inspired the hypothesis that kilometer-scale ice sheets provided the confining pressure for sand injection (44). Injectite emplacement was likely promoted by seismicity associated with basement fracturing and faulting during regional Neoproterozoic extension associated with Rodinia supercontinent breakup (44) as manifested by injection of dikes up to 7 m in width (*SI Appendix*, Fig. S2) along the extensional Ute Pass fault. Still earlier exposure of the granite to surface weathering is consistent with fragments of weathered Pikes Peak granite entrained in unweathered injectites (Fig. 3*C* and *SI Appendix*, Fig. S3 *A* and *B*). The cold conditions that prevailed during the 717- to 660-Ma Sturtian glaciations were not conducive to regolith development. If the injectites formed during the >639- to 635-Ma Marinoan glaciation, a regolith could have formed between ∼660 and 640 Ma, but a 640- to 635-Ma age of the injectites seems inconsistent with the existing geochronology. This suggests a minimum age of 717 Ma for weathering of the granite and therefore, for basement exhumation to the surface.

In our study area, the Cambrian Sawatch sandstone overlies Tavakaiv-injected Pikes granite, thus indicating little basement exhumation between Cryogenian and Cambrian times. If substantial exhumation had occurred, then the shallowly emplaced injectites would have been removed by erosion. Although in the southern part of the batholith the Tavakaiv and Sawatch occur on opposite sides of the Ute Pass fault, farther north at Perry Park the Sawatch sits directly on Tavakaiv-injected granite (Fig. 2). Locally, the basal Cambrian beds above the Great Unconformity drape over relief induced by variably resistant, meter-scale core stones in an ∼100-m-thick weathered zone of the Pikes Peak granite (Fig. 3*A*). This is clear evidence that a Pikes granite regolith was also present in the Cambrian. Although the Pikes Peak batholith was later buried and reexhumed multiple times in the Phanerozoic, the Tavakaiv injectites provide evidence for initial granite exposure and development of the Great Unconformity erosion surface by 717 Ma.

Constraints on the Great Unconformity in Colorado from Zircon (U-Th)/He Thermochronology

Although the geologic information alone requires Pikes Peak basement exposure prior to Cryogenian Tavakaiv sediment accumulation and sand injection, we additionally acquired (U-Th)/He thermochronology data for 30 individual zircon crystals from five Pikes Peak granite samples proximal to the Neoproterozoic and Cambrian paleosurfaces in an effort to refine the timing of initial basement exhumation (*Materials and Methods*). Rocks cool as they are exhumed to the surface, and ZHe data can record key portions of this cooling history. Three of our samples (PP1 to PP3) were collected on the eastern side of Pikes Peak on the footwall (western side) of the Ute Pass fault (Fig. 2). The closest identified Tavakaiv injectite exposures are in the footwall, ∼800 m east of the easternmost of these samples (PP1). Two of our samples are located immediately below the Great Unconformity where it is overlain by the Cambrian Sawatch sandstone (Fig. 2). One of these samples (F1936) was collected ∼10 m below the sandstone where the Sawatch overlies core stones in the Pikes Peak basement (Fig. 3*A*) on the downthrown (eastern side) of the Ute Pass fault, ∼800 m northeast of sample PP1. The other sample (F1937) was collected ∼2 m below the Great Unconformity (Fig. 3*D*) where the Sawatch overlies Tavakaiv-injected Pikes Peak basement, located ∼43 km north of F1936 in Perry Park. Zircon data from all samples display similar negative correlations between ZHe date and effective uranium concentration (eU), with dates ranging from 975 ± 41 to 46 ± 1 Ma over an eU span of 37 to 1,955 ppm (Fig. 4*A* and *SI Appendix*, Table S1). This pattern is consistent with lower He retentivity at higher radiation damage dose (*Materials and Methods*). The dates do not vary with grain size (*SI Appendix*, Fig. S4). Intracrystalline eU zonation likely contributes to ZHe data dispersion beyond what can be accounted for by variability in bulk eU and crystal size (47–49).

We carried out tT (time–temperature) simulations of the Pikes Peak ZHe data using the HeFTy program (50) and a zircon radiation damage accumulation and annealing model (ZRDAAM) (51) to test for compatibility of the ZHe data with the geologic evidence for pre–717-Ma basement exhumation. Full model details are in *Materials and Methods* and *SI Appendix*, Table S2 (52). Model results are in Fig. 4*B*. The "best-fit" tT trajectory reproduces the observed ZHe date–eU pattern (Fig. 4*A*, dashed curve). The key result is that, following shallow batholith emplacement and initial rapid cooling, the suite of viable tT paths allows cooling and exhumation to surface conditions anytime between ∼1000 and 717 Ma. This outcome is thus consistent with the geologic evidence for pre–717-Ma basement exhumation and development of the Great Unconformity erosion surface.

Discussion

Development of the Great Unconformity Erosion Surface in Colorado before Neoproterozoic Snowball Earth. Our geologic and thermochronologic results provide evidence that the ∼1.07-Ga Pikes Peak batholith was exhumed and first exposed to weathering between ∼1000 and 717 Ma, which led to development of the Great Unconformity paleosurface. This indicates that most exhumation below the Great Unconformity in Colorado occurred before the Sturtian glaciation and favors either Rodinia supercontinent assembly before 850 Ma (Hypothesis 1) and/or Rodinia breakup between 850 and 717 Ma (Hypothesis 2) as the cause(s) (Fig. 1). Rodinia formed during the terminal Mesoproterozoic Grenville orogeny and rifted apart from ca. 850 to 700 Ma (53–55). Grenville orogenesis produced Late Mesoproterozoic topography and magmatism across Laurentia from southeastern Canada (56, 57) through the midcontinent (58) to the American

Southwest (59). Mantle convection models suggest that a ring of subduction around the fully assembled Rodinia would have caused bipolar upwelling before 800 Ma (17), with the thick supercontinent crust creating a thermal lid, inducing Late Mesoproterozoic to Early Tonian intraplate magmatism throughout Rodinia (14, 60). In our study area, these processes could have induced Pikes Peak batholith magmatism, surface uplift, and erosion (Hypothesis 1). Early Rodinia breakup along the Cordilleran margin associated with the Gunbarrel large igneous province (61) and Late Tonian basin formation (62, 63) also is a feasible mechanism for exhumation. Neoproterozoic normal faulting along the Ute Pass fault (64) as well as detrital zircon age distributions in Tavakaiv sandstone that resemble those of the Chuar–Uinta Mountains–Pahrump and Cryogenian basins across the western United States are consistent with intracontinental extension in the Pikes region in Cryogenian time (43, 44, 64), which may have exhumed the basement to the surface (Hypothesis 2).

Other recent thermochronologic work also constrains Neoproterozoic cooling and denudation events. K-feldspar $^{40}Ar/^{39}Ar$ multidiffusion domain data from the southern Canadian shield record significant post–1.0-Ga cooling attributed to exhumation associated with magmatic underplating during Midcontinent Rift extension and Grenville orogenesis (56). ZHe data from the Ozark Plateau of the US midcontinent (16) as well as data from uplifts in the Wyoming craton (28) were used to decipher Neoproterozoic cooling and erosion that overlaps with Rodinia supercontinent breakup. Titanite and zircon (U-Th)/He data from southern Africa indicate substantial ∼1.1-Ga burial of the Kaapvaal craton during Rodinia assembly and imply Neoproterozoic cooling and erosion (65). However, none of these investigations require an age for the Great Unconformity erosion surface older than the Sturtian Snowball Earth as necessitated by the geological relationships in the Pikes Peak region. Instead, Precambrian rocks in the Ozark Plateau and Wyoming, southern Canadian shield, and Kaapvaal craton are overlain by Cambrian, upper Ordovician, or Carboniferous units, respectively. These relationships and the thermochronologic data impose Paleozoic minimum ages on erosion surface development at these locations in contrast to the 717-Ma minimum age bound in our study. Consequently, our dataset is the only one that allows for discrimination among any of the hypotheses in Fig. 1.

As an example, we carried out thermal history simulations of the published ZHe data from the Ozark Mountains of the central United States (16) to compare how well the timing of Great Unconformity erosion surface formation in the Ozarks is resolved relative to our Pikes Peak study region. We applied the same geologic constraints as in ref. 16, with full model details in *Materials and Methods* and *SI Appendix*, Table S3. We find that the good-fit tT paths for the Ozark data allow basement exhumation to the surface anytime between 957 and 511 Ma, with major cooling to <100 °C permitted as early as 1037 Ma and as late as 600 Ma (*SI Appendix*, Fig. S5 *A* and *B*). This outcome is far less restrictive than our Pikes Peak result, which is due to Cambrian rather than Cryogenian geologic relationships imposing the minimum age on Great Unconformity development in the Ozarks (*SI Appendix*, Fig. S5 *B* and *C*). This highlights the value of paleosurface observations for determining the Great Unconformity's age at the level required to differentiate among the hypotheses for its origin as enabled by the Cryogenian Tavakaiv injectite relationships in the Pikes Peak region.

Limited Erosion during Neoproterozoic Snowball Earth. Our dataset from Pikes Peak indicates that most erosion below the Great Unconformity occurred before the onset of the Sturtian Snowball Earth here, with limited basement denudation between 717 Ma and deposition of the Sawatch sandstone at 510 Ma. The Tavakaiv injectites were emplaced in both the immediate subsurface and up to depths of <1 km (42) such that their regional preservation and occurrence below the Sawatch indicates <1 km of cumulative Pikes granite erosion between Tavakaiv injection and Sawatch deposition. If the ∼100-m-thick weathered zone with core stones under the Sawatch (Fig. 3*A*) is the same regolith intruded by the Tavakaiv injectites, then net denudation was as little as <100 m from 717 to 510 Ma, which encompasses both Cryogenian Snowball Earth events and Ediacaran glaciations.

This direct evidence from our study area for limited denudation during the Neoproterozoic glaciations is at odds with recent work that indirectly inferred a global average of 3 to 5 km of erosion during this interval based primarily on preserved sediment volumes in North America (i.e., Macrostrat), isotopic proxy data (zircon εHf and O isotopes), and the impact cratering record (2). This proposed massive erosion event is inconsistent not only with our observational data but also with other geologic constraints on North America indicating far less than 3 to 5 km of Cryogenian erosion. These include preservation of >1 km of ca. 720-Ma basalt in the Natkusiak Formation of northwest Canada (66); >450 m of ca. 720-Ma basalt in the Kikiktak Formation of Arctic Alaska (67); and 780- to 717-Ma sedimentary basins in Grand Canyon, in Death Valley, in the Uinta Mountains of Utah, throughout the Canadian Cordillera (63), and in the central Appalachians (68). Moreover, sedimentation rates on the continental margins were anomalously low during the Cryogenian (69), indicating reduced rather than increased erosion of the continents. Thus, the geologic observations and available thermochronologic data do not support a single immense, worldwide denudation episode during the Neoproterozoic Snowball Earth.

Diachronous Tectonic Origin of Great Unconformities. In contrast to the notion that Great Unconformity erosion was a synchronous global phenomenon (2, 4, 5), we propose that it was diachronous and in places, composite, such that multiple Great Unconformities were generated by more than one denudational episode with tectonic causes that varied geographically. During the Neoproterozoic, different continental margins were variably affected by collisional tectonism and rifting during Rodinia and Pannotia/Gondwana assembly and breakup. For example, on the North American margins, there is not one Great Unconformity characterized by a single set of relationships, but rather there is a composite surface with overlapping unconformities that encompasses multiple stages of Rodinia and Pannotia rifting (27, 63, 70–72). The Appalachian margin was affected by the extensive Grenvillian orogenic system while the Cordilleran margin was not; the former saw Ediacaran magmatism and rifting while the latter underwent extension and rift-related volcanism primarily in the Tonian to Cryogenian. On other continents, such as the Kalahari craton and across much of Africa, widespread unconformities are overlain by Late Neoproterozoic and Cambrian strata that formed in foreland basins associated with the Pan-African orogeny (73). Thus, we suggest that sub-Great Unconformity erosion occurred at different times and for different reasons in different places, generating multiple Great Unconformities. Our results resolve a pre-Sturtian Snowball Earth age for the Great Unconformity erosion surface in one region of North America. Additional direct constraints on the age, duration, and spatial extent of Great Unconformity formative events elsewhere are required to develop a global understanding of the Great Unconformities and their significance.

Conclusions

Our study documents that the majority of erosion below the Great Unconformity at Pikes Peak predates the Sturtian-age Tavakaiv injectites. This result is inconsistent with recent proposals that the Great Unconformity formed in a single global

exhumation pulse during the Neoproterozoic Snowball Earth (2) and is responsible for a putative transition to modern tectonics (3). Rather, we propose that there are multiple, regionally diachronous Great Unconformities with tectonic origins. Although the relationships suggest that Neoproterozoic glacial erosion did not singularly generate the Great Unconformity, it is possible that Rodinia rifting increased global weatherability and created the tectonic context for the initiation of Snowball Earth (11, 15, 16). If the Great Unconformities are a worldwide phenomenon, it must relate to the Tonian removal of topography generated in the assembly of Rodinia, with erosion and sedimentation histories diverging during diachronous and prolonged Late Neoproterozoic supercontinent breakup and glaciation.

Materials and Methods

Zircon (U-Th)/He Thermochronology. (U-Th)/He thermochronology is based on the radioactive decay of trace U and Th (and to a lesser extent, Sm) to ^{4}He in a mineral's structure and on thermally controlled volume diffusion of the ^{4}He atoms. At high temperatures, He escapes from the crystal, while at low temperatures, it is retained. The temperature range for He retention depends on the mineral's He diffusion kinetics, which is influenced by crystal lattice structure, grain size (74), and radiation damage (51, 75–77). Parent–isotope zonation (48–50), He injection from neighboring phases (78), and grain fragmentation (79) are additional factors that can influence (U-Th)/He data.

In zircon, radiation damage exerts strong control on He retentivity and the associated data patterns. Damage accumulation initially causes the He closure temperature (T_c) to increase from ∼140 °C to 220 °C, but after a damage percolation threshold is surpassed, the T_c progressively decreases to <50 °C (51, 80). Heating can anneal radiation damage, which in turn, affects He retentivity (76, 80). For zircon suites with a shared thermal history and a span of U-Th, radiation damage can generate positive or negative correlations between ZHe date and eU (eU = U + 0.235 × Th) (51). These patterns develop if the tT history is characterized by enough time for damage accumulation and development of variable He retentivities in a mineral suite followed by reheating, partial resetting, and/or protracted cooling through the mineral's partial retention zone (81). However, even if the mineral suite develops variable He retentivities, tT paths with only rapid cooling and/or reheating and complete resetting will not induce date–eU correlations (81).

A zircon radiation damage accumulation and annealing model (ZRDAAM) (51) is available that allows for quantitative thermal history interpretation of ZHe datasets. The high-damage end of the ZRDAAM is least well constrained (51, 82, 83). Recent work shows that bulk radiation damage annealing in zircon requires hotter temperatures for longer intervals than assumed by the fission track annealing model currently used by the ZRDAAM (84). Active research is underway by different groups to improve understanding of zircon He diffusion and radiation damage annealing.

Zircon crystals were isolated from the samples using standard crushing, water table, heavy-liquid, and magnetic separation techniques. Individual crystals were handpicked for analysis based on crystal shape, size, and color using a Leica M164 binocular microscope equipped with both polarized transmitted and reflected light. Zircons were specifically selected to have a range of opacity and discoloration, with the goal of analyzing crystals that encompass a broad range of radiation damage (85). Grains were photographed, measured, packed into HCl-cleaned Nb packets, and analyzed for He using an ASI Alphachron He extraction and measurement line in the University of Colorado Boulder Thermochronology Research and Instrumentation Laboratory (CU TRaIL). Degassed crystals were then retrieved, spiked with a calibrated ^{235}U-^{230}Th-^{145}Nd tracer, and dissolved using pressurized, high-temperature HF-HCl acid–vapor dissolution vessels. Dissolved samples were measured for U, Th, and Sm on either an Agilent 7900 quadrupole inductively coupled plasma-mass spectrometer (ICP-MS) in the CU TRaIL or a Thermo-Finnigan Element2 sector field ICP-MS.

The ^{4}He atoms travel up to 20 μm during α-decay, requiring that a correction be applied based on crystal size and geometry to account for He lost owing to this effect. Standard α-ejection corrections were made using the approach of ref. 86. Crystal volumes used to compute isotopic concentrations were also calculated using the idealized crystal morphologies of ref. 86. We assign a conservative 15% uncertainty to eU values to account for observed variations from ideal geometries using the approach of ref. 77. Uncertainties on individual ZHe dates are reported at 2σ and are based on the propagated analytical uncertainties on the U, Th, and He measurements.

All data are available in *SI Appendix*, Table S1.

Thermal History Modeling of the Zircon (U-Th)/He Data. We simulated the Pikes Peak ZHe data using the HeFTy program (50) and the ZRDAAM (51). The imposed thermal history constraints (thick green boxes in Fig. 4*B*) include 1) shallow emplacement of the Pikes Peak batholith at 1.07 Ga (31) followed by rapid cooling based on hornblende, biotite, and K-feldspar ^{40}Ar/^{39}Ar data (33); 2) attainment of surface conditions prior to the Sturtian glaciation at 717 Ma, maximum temperatures of 30 °C during the Snowball glaciations based on equatorial ice sheet thicknesses of 0 to 3 km in Snowball Earth climate models (87) and the position of Colorado at or near the equator during this time (88), and surface conditions by the onset of 510-Ma Sawatch sandstone deposition above the Great Unconformity (24); 3) early Paleozoic burial heating followed by surface conditions by the time of deposition of the Pennsylvanian Fountain Formation on the Pikes Peak granite; and 4) post–300-Ma burial heating with surface conditions by 64 Ma based on the occurrence of Pikes Peak granite clasts in the Arapahoe Formation (37). We applied a near-surface "exploration field" box between Pikes Peak granite emplacement and surface conditions at 717 Ma that did not restrict the models but ensured that this regime of tT space was fully tested.

The models simulate random tT paths forced through the geologically defined tT constraints but otherwise explore the full model tT space. The ZHe data from all of the Pikes Peak granite samples were split into four eU–date bins, with the mean values for the ZHe date, eU, and equivalent spherical radius of each bin used as model inputs. Paths are considered "good" or "acceptable" if they reproduce the input data to specified statistical thresholds (*SI Appendix*, Table S2) (50, 89). The results indicate cooling to surface temperatures between ∼1000 and 717 Ma, demonstrating that the ZHe data are consistent with basement exhumation to the surface before 717 Ma. We emphasize that the key conclusion of pre–717-Ma development of the sub-Great Unconformity erosion surface is derived from the Cryogenian Tavakaiv injectite relationships, and thus, it is independent of the ZHe data and any shortcomings of the ZRDAAM.

We also simulated the published ZHe data (16) from the Ozark Mountains of the central United States to evaluate how well those results resolve the timing of erosion below the Great Unconformity compared with our data from Pikes Peak (*SI Appendix*, Fig. S5 *A* and *B*). We again used inverse modeling with the HeFTy program (50) and the ZRDAAM (51). We applied the same geologic constraints as in ref. 16 (full details are in *SI Appendix*, Table S3), which include 1) granite crystallization at 1.47 to 1.38 Ga at temperatures of 600 °C to 550 °C followed by cooling to the surface by 1.35 Ma based on volcanics of this age overlying the basement, 2) allowing burial reheating between 1350 and 510 Ma to temperatures sufficient to reset the ZHe data followed by surface conditions by the onset of 509-Ma Lamotte sandstone deposition above the Great Unconformity, 3) Paleozoic burial reheating to account for deposition of Paleozoic sedimentary rocks in the region, 4) temperatures <120 °C after 209 Ma based on AFT dates of 209 to 185 Ma, and 5) surface conditions today. We imposed a constraint box for the AFT data because the full AFT date and track-length data were not published, and therefore we are unable to model them. We applied a near-surface exploration field for the 500-My preceding surface conditions at 509 Ma that did not restrict the models but ensured that this regime of tT space was fully tested. It seems that this exploration box was not imposed in the models reported in ref. 16. We suspect that the omission of this box caused the models in ref. 16 to not fully explore this key region of tT space and to yield results that artificially suggest a more restricted interval of pre-Great Unconformity erosional cooling than constrained by the data in reality.

The ZHe data from all four samples were split into five eU–date bins, with the mean values for the ZHe date, eU, and equivalent spherical radius of each bin used as model inputs. We additionally included the apatite (U-Th)/He data from sample 14OZ11 in this simulation and used the apatite radiation damage and accumulation model for He diffusion kinetics (81). We simulated this sample because the apatite (U-Th)/He data are reproducible, unlike the dispersed results for sample 14OZ12. *SI Appendix*, Fig. S5*B* shows the results of this thermal history simulation. The important outcome is that the data allow basement exhumation to the surface at any time between 957 and 511 Ma prior to deposition of Cambrian sandstone above the Great Unconformity. This result is far less restrictive than that in our Pikes Peak study, where the observations and data require that the basement below the Great Unconformity was exhumed to the surface between ∼1000 and 717 Ma (*SI Appendix*, Fig. S5 *B* and *C*).

ACKNOWLEDGMENTS. This work was supported by NSF Division of Earth Sciences Grants 1759200 and 1916698 (to R.M.F. and F.A.M.). NSF Division of Earth Sciences Grants 1126991 and 1559306 (to R.M.F.) provided support for the CU TRaIL instrumentation used to acquire the ZHe data. We thank Jim Metcalf for assistance obtaining the (U-Th)/He results. We appreciate the helpful reviews provided by two anonymous reviewers that improved the clarity of the manuscript.

1. C. R. Darwin, *On the Origin of Species* (John Murray Publishing, London, UK, 1859).
2. C. B. Keller *et al*., Neoproterozoic glacial origin of the Great Unconformity. *Proc. Natl. Acad. Sci. U.S.A.* **116**, 1136–1145 (2019).
3. S. V. Sobolev, M. Brown, Surface erosion events controlled the evolution of plate tectonics on Earth. *Nature* **570**, 52–57 (2019).
4. J. M. Husson, S. E. Peters, Atmospheric oxygenation driven by unsteady growth of the continental sedimentary reservoir. *Earth Planet. Sci. Lett.* **460**, 68–75 (2017).
5. S. E. Peters, R. R. Gaines, Formation of the 'Great Unconformity' as a trigger for the Cambrian explosion. *Nature* **484**, 363–366 (2012).
6. L. Sloss, "Tectonic volution of the craton in Phanerozoic time" in *The Geology of North America: An Overview,* A. W. Bally, A. R. Palmer, Eds. (Geological Society of America, McLean, VA, 1988), Vol. 2, pp. 25–51.
7. P. F. Hoffman *et al*., Snowball Earth climate dynamics and Cryogenian geology-geobiology. *Sci. Adv.* **3**, e1600983 (2017).
8. A. C. Maloof *et al*., The earliest Cambrian record of animals and ocean geochemical change. *Geol. Soc. Am. Bull.* **122**, 1731–1774 (2010).
9. S. Xiao *et al*., Towards an Ediacaran time scale: Problems, protocols, and prospects. *Episodes* **39**, 540–555 (2016).
10. G. M. Cox *et al*., Continental flood basalt weathering as a trigger for Neoproterozoic Snowball Earth. *Earth Planet. Sci. Lett.* **446**, 89–99 (2016).
11. Y. Godderis *et al*., The Sturtian 'snowball' glaciation: Fire and ice. *Earth Planet. Sci. Lett.* **211**, 1–12 (2003).
12. G. P. Halverson, F. O. Dudás, A. C. Maloof, S. A. Bowring, Evolution of the $^{87}Sr/^{86}Sr$ composition of Neoproterozoic Seawater. *Palaeogeogr. Palaeoclimatol. Palaeoecol.* **256**, 103–129 (2007).
13. F. Horton, Did phosphorus derived from the weathering of large igneous provinces fertilize the Neoproterozoic ocean? *Geochem. Geophys. Geosyst.* **16**, 1723–1738 (2015).
14. Z.-X. Li, S. Zhong, Supercontinent–superplume coupling, true polar wander and plume mobility: Plate dominance in whole-mantle tectonics. *Phys. Earth Planet. Inter.* **176**, 143–156 (2009).
15. F. A. Macdonald *et al*., Calibrating the Cryogenian. *Science* **327**, 1241–1243 (2010).
16. M. DeLucia, W. Guenthner, S. Marshak, S. Thomson, A. Ault, Thermochronology links denudation of the Great Unconformity surface to the supercontinent cycle and Snowball Earth. *Geology* **46**, 167–170 (2017).
17. S. Zhong, N. Zhang, Z.-X. Li, J. H. Roberts, Supercontinent cycles, true polar wander, and very long-wavelength mantle convection. *Earth Planet. Sci. Lett.* **261**, 551–564 (2007).
18. S. K. Sahoo *et al*., Ocean oxygenation in the wake of the Marinoan glaciation. *Nature* **489**, 546–549 (2012).
19. K. V. Lau, F. A. Macdonald, K. Maher, J. L. Payne, Uranium isotope evidence for temporary ocean oxygenation in the aftermath of the Sturtian Snowball Earth. *Earth Planet. Sci. Lett.* **458**, 282–292 (2017).
20. P. A. Pogge von Strandmann *et al*., Selenium isotope evidence for progressive oxidation of the Neoproterozoic biosphere. *Nat. Commun.* **6**, 10157 (2015).
21. J. J. Brocks *et al*., The rise of algae in Cryogenian oceans and the emergence of animals. *Nature* **548**, 578–581 (2017).
22. N. J. Planavsky *et al*., The evolution of the marine phosphate reservoir. *Nature* **467**, 1088–1090 (2010).
23. M. Brasier, The Lower Cambrian transgression and glauconite-phosphate facies in western Europe. *J. Geol. Soc.* **137**, 695–703 (1980).
24. K. Karlstrom *et al*., Cambrian Sauk transgression in the Grand Canyon region redefined by detrital zircons. *Nat. Geosci.* **11**, 438–443 (2018).
25. R. A. Squire, I. H. Campbell, C. M. Allen, C. J. L. Wilson, Did the Transgondwanan supermountain trigger the exposive radiation of animals on Earth? *Earth Planet. Sci. Lett.* **250**, 116–133 (2006).
26. R. D. Nance, J. B. Murphy, Supercontinents and the case for Pannotia. *Geol. Soc. Lond. Spec. Publ.* **470**, 65–86 (2018).
27. K. E. Karlstrom, J. M. Timmons, "Many unconformities make one 'Great Unconformity'" in *Grand Canyon Geology: Two Billion Years of Earth's History*, K. E. Karlstrom, J. M. Timmons, Eds. (Geological Society of America, McLean, VA, 2012), vol. 489, pp. 73–79.
28. D. A. Orme, W. R. Guenthner, A. K. Laskowski, P. W. Reiners, Long-term tectonothermal history of Laramide basement from zircon–He age-eU correlations. *Earth Planet. Sci. Lett.* **453**, 119–130 (2016).
29. O. Tweto, *Rock Units of the Precambrian Basement in Colorado: Usgs Professional Paper 1321-A* (BiblioGov, 1987), p. 54.
30. D. R. Smith *et al*., Petrology and geochemistry of late-stage intrusions of A-type, mid-Proterozoic Pikes Peak batholith (Central Colorado, USA); implications for petrogenetic models. *Precambrian Res.* **98**, 271–305 (1999).
31. M. Guitreau, S. B. Mukasa, J. Blichert-Toft, M. F. Fahnestock, Pikes Peak batholith (Colorado, USA) revisited: A SIMS and LA-ICP-MS study of zircon U–Pb ages combined with solution Hf isotopic compositions. *Precambrian Res.* **280**, 179–194 (2016).
32. F. Barker, D. Wones, W. Sharp, G. Desborough, The Pikes Peak batholith, Colorado Front Range, and a model for the origin of the gabbro—anorthosite—syenite—potassic granite suite. *Precambrian Res.* **2**, 97–160 (1975).
33. D. Unruh, L. Snee, E. Foord, W. Simmons, "Age and cooling history of the Pikes Peak batholith and associated pegmatites" in *GSA Abstracts with Programs*, (Geological Society of America, Boulder, CO, 1995), p. 468.
34. S. Kelley, C. Chapin, S. Cather, Denudation history and internal structure of the Front Range and Wet Mountains, Colorado, based on apatite-fission-track thermochronology. *N. M. Bur. Geol. Miner. Resour.* **160**, 41–77 (2004).
35. C. Naeser *et al*., "Tertiary cooling and tectonic history of the White River Uplift, Gore Range, and Western Front Range, central Colorado: Evidence from fission-track and 39Ar/40Ar ages" in *Late Cenozoic Evaporite Tectonism and Volcanism in West-Central Colorado*, R. M. Kirkham, R. B. Scott, T. W. Judkins, Eds. (Geological Society of America, Boulder, CO, 2002), vol. 366, pp. 31–54.
36. L. J. Suttner, R. P. Langford, A. F. O'Connell, *New Interpretation of the Stratigraphic Relationship between the Fountain Formation and Its Glen Eyrie Member* (Rocky Mountain Section [SEPM], 1984).
37. C. F. Kluth, S. N. Nelson, Age of the Dawson arkose, southwestern air force academy, Colorado, and implications for the uplift history of the front range. *Mt. Geol.* **25**, 29–35 (1988).
38. R. J. Weimer, S. A. Sonnenberg, *Guide to the Petroleum Geology and Laramide Orogeny, Denver Basin and Front Range, Colorado* (Colorado Geological Survey, Department of Natural Resources, 1996).
39. G. R. Scott, *Bedrock Geology of the Kassler Quadrangle, Colorado* (US Government Printing Office, 1963).
40. M. Morgan *et al*., "Geologic map of the cascade quadrangle" (Tech. Rep. Open File Report: 03-18, El Paso County, Colorado Geological Survey, Denver, CO, 2003).
41. J. Keller *et al*., "Geologic map of the Manitou Springs 7.5-minute quadrangle" (Tech. Rep. Open File Report: 03-19, El Paso and Teller Counties, Colorado Geological Survey, Denver, CO, 2005).
42. C. Siddoway, G. Palladino, G. Prosser, D. Freedman, W. Duckworth, Basement-hosted sand injectites: Use of field examples to advance understanding of hydrocarbon reservoirs in fractured crystalline basement rocks. *Geol. Soc. Lond. Spec. Publ.*, 10.1144/SP493-2018-140 (2019).
43. C. S. Siddoway, G. E. Gehrels, Basement-hosted sandstone injectites of Colorado: A vestige of the Neoproterozoic revealed through detrital zircon provenance analysis. *Lithosphere* **6**, 403–408 (2014).
44. J. L. Jensen *et al*., Single-crystal hematite (U–Th)/He dates and fluid inclusions document widespread Cryogenian sand injection in crystalline basement. *Earth Planet. Sci. Lett.* **500**, 145–155 (2018).
45. A. D. Rooney *et al*., Re-Os geochronology and coupled Os-Sr isotope constraints on the Sturtian snowball Earth. *Proc. Natl. Acad. Sci. U.S.A.* **111**, 51–56 (2014).
46. A. D. Rooney, J. V. Strauss, A. D. Brandon, F. A. Macdonald, A Cryogenian chronology: Two long-lasting synchronous Neoproterozoic glaciations. *Geology* **43**, 459–462 (2015).
47. J. K. Hourigan, P. W. Reiners, M. T. Brandon, U-Th zonation-dependent alpha-ejection in (U-Th)/He chronometry. *Geochim. Cosmochim. Acta* **69**, 3349–3365 (2005).
48. M. Danišík *et al*., Seeing is believing: Visualization of He distribution in zircon and implications for thermal history reconstruction on single crystals. *Sci. Adv.* **3**, e1601121 (2017).
49. K. Farley, D. Shuster, R. A. Ketcham, U and Th zonation in apatite observed by laser ablation ICPMS, and implications for the (U–Th)/He system. *Geochim. Cosmochim. Acta* **75**, 4515–4530 (2011).
50. R. A. Ketcham, Forward and inverse modeling of low-temperature thermochronometry data. *Rev. Mineral. Geochem.* **58**, 275–314 (2005).
51. W. R. Guenthner, P. W. Reiners, R. A. Ketcham, L. Nasdala, G. Giester, Helium diffusion in natural zircon: Radiation damage, anisotropy, and the interpretation of zircon (U-Th)/He thermochronology. *Am. J. Sci.* **313**, 145–198 (2013).
52. R. M. Flowers, K. A. Farley, R. A. Ketcham, A reporting protocol for thermochronologic modeling illustrated with data from the Grand Canyon. *Earth Planet. Sci. Lett.* **432**, 425–435 (2015).
53. Z. X. Li *et al*., Assembly, configuration, and break-up history of Rodinia: A synthesis. *Precambrian Res.* **160**, 179–210 (2008).
54. E. M. Moores, Southwest US-East Antarctic (SWEAT) connection: A hypothesis. *Geology* **19**, 425–428 (1991).
55. P. F. Hoffman, Did the breakout of laurentia turn gondwanaland inside-out? *Science* **252**, 1409–1412 (1991).
56. K. T. McDannell, P. K. Zeitler, D. Schneider, Instability of the southern Canadian shield during the late proterozoic. *Earth Planet. Sci. Lett.* **490**, 100–109 (2018).
57. M. M. Streepey, C. Lithgow-Bertelloni, B. A. van der Pluijm, E. J. Essene, J. F. Magloughlin, "Exhumation of a collisional orogen: A perspective from the North American Grenville province" in *Proterozoic Tectonic Evolution of the Grenville Orogen in North America*, R. P. Tollo, L. Corriveau, J. McLelland, and M. J. Bartholomew, Eds. (Geological Society of America Memoir 197, Geological Society of America, Boulder, CO, 2004), pp. 391–410.
58. N. L. Swanson-Hysell, J. Ramezani, L. M. Fairchild, I. R. Rose, Failed rifting and fast drifting: Midcontinent rift development, Laurentia's rapid motion and the driver of Grenvillian orogenesis. *GSA Bulletin* **131**, 913–940 (2019).
59. R. M. Bright *et al*., U-Pb geochronology of 1.1 Ga diabase in the southwestern United States: Testing models for the origin of a post-Grenville large igneous province. *Lithosphere* **6**, 135–156 (2014).
60. R. E. Hanson *et al*., Coeval large-scale magmatism in the Kalahari and Laurentian cratons during Rodinia assembly. *Science* **304**, 1126–1129 (2004).
61. S. S. Harlan, L. M. Heaman, A. N. LeCheminant, W. R. Premo, Gunbarrel mafic magmatic event: A key 780 Ma time marker for Rodinia plate reconstructions. *Geology* **31**, 1053–1056 (2003).
62. W. Yonkee *et al*., Tectono-stratigraphic framework of Neoproterozoic to Cambrian strata, west-central US: Protracted rifting, glaciation, and evolution of the North American Cordilleran margin. *Earth Sci. Rev.* **136**, 59–95 (2014).
63. C. Dehler *et al*., Synthesis of the 780–740 Ma Chuar, Uinta Mountain, and Pahrump (ChUMP) groups, western USA: Implications for Laurentia-wide cratonic marine basins. *Geol. Soc. Am. Bull.* **129**, 607–624 (2017).
64. C. Siddoway, P. Myrow, E. Fitz-Díaz, "Strata, structures, and enduring enigmas: A 125th anniversary appraisal of Colorado Springs geology" in *Classic Concepts and New Directions: Exploring 125 Years of GSA Discoveries in the Rocky Mountain Region*, L. D. Abbott, G. S. Hancock, Eds. (Geological Society of America, Boulder, CO, 2013), vol. 33, pp. 331–356.

65. J. S. Baughman, R. M. Flowers, Mesoproterozoic burial of the Kaapvaal craton, southern Africa during Rodinia supercontinent assembly from (U-Th)/He thermochronology. *Earth Planet. Sci. Lett.* **531**, 115930 (2020).
66. C. W. Jefferson, W. E. Nelson, R. V. Kirkhm, J. H. Reedman, R. F. J. Scoates, *Geology and Copper Occurrences of the Natkusiak Basalts, Victoria Island, District of Franklin. Current Research Part A* (Geological Survey of Canada, 1985), pp. 203–214.
67. G. M. Cox *et al*., Kikiktat volcanics of Arctic Alaska—melting of harzburgitic mantle associated with the Franklin large igneous province. *Lithosphere* **7**, 275–295 (2015).
68. A. J. Merschat *et al*., "Key structural and stratigraphic relationships from the northeast end of the Mountain City window and the Mount Rogers area, Virginia–North Carolina–Tennessee" in *Elevating Geoscience in the Southeastern United States: New Ideas about Old Terranes: Field Guides for the GSA Southeastern Section Meeting, Blacksburg, Virginia, 2014*, C. M. Bailey, L. V. Coiner, Eds. (Geological Society of America, Denver, CO, 2014), vol. 35, pp. 63–101.
69. C. A. Partin, P. M. Sadler, Slow net sediment accumulation sets Snowball Earth apart from all younger glacial episodes. *Geology* **44**, 1019–1022 (2016).
70. F. A. Macdonald *et al*., The Laurentian record of Neoproterozoic glaciation, tectonism, and eukaryotic evolution in Death Valley, California. *Geol. Soc. Am. Bull.* **125**, 1203–1223 (2013).
71. F. A. Macdonald *et al*., The stratigraphic relationship between the Shuram carbon isotope excursion, the oxygenation of Neoproterozoic oceans, and the first appearance of the Ediacara biota and bilaterian trace fossils in northwestern Canada. *Chem. Geol.* **362**, 250–272 (2013).
72. J. P. Smoot, S. Southworth, Volcanic rift margin model for the rift-to-drift setting of the late Neoproterozoic-early Cambrian eastern margin of Laurentia: Chilhowee group of the Appalachian Blue Ridge. *Geol. Soc. Am. Bull.* **126**, 201–218 (2014).
73. G. J. Germs, The Neoproterozoic of southwestern Africa, with emphasis on platform stratigraphy and paleontology. *Precambrian Res.* **73**, 137–151 (1995).
74. P. W. Reiners, K. A. Farley, Influence of crystal size on apatite (U–Th)/He thermochronology: An example from the Bighorn Mountains, Wyoming. *Earth Planet. Sci. Lett.* **188**, 413–420 (2001).
75. R. Flowers, D. Shuster, B. Wernicke, K. Farley, Radiation damage control on apatite (U-Th)/He dates from the Grand Canyon region, Colorado Plateau. *Geology* **35**, 447–450 (2007).
76. D. L. Shuster, K. A. Farley, The influence of artificial radiation damage and thermal annealing on helium diffusion kinetics in apatite. *Geochim. Cosmochim. Acta* **73**, 183–196 (2009).
77. J. S. Baughman, R. M. Flowers, J. R. Metcalf, T. Dhansay, Influence of radiation damage on titanite He diffusion kinetics. *Geochim. Cosmochim. Acta* **205**, 50–64 (2017).
78. K. E. Murray, D. A. Orme, P. W. Reiners, Effects of U–Th-rich grain boundary phases on apatite helium ages. *Chem. Geol.* **390**, 135–151 (2014).
79. R. W. Brown *et al*., Natural age dispersion arising from the analysis of broken crystals. Part I. Theoretical basis and implications for the apatite (U–Th)/He thermochronometer. *Geochim. Cosmochim. Acta* **122**, 478–497 (2013).
80. R. A. Ketcham, W. R. Guenthner, P. W. Reiners, Geometric analysis of radiation damage connectivity in zircon, and its implications for helium diffusion. *Am. Mineral.* **98**, 350–360 (2013).
81. R. M. Flowers, R. A. Ketcham, D. L. Shuster, K. A. Farley, Apatite (U–Th)/He thermochronometry using a radiation damage accumulation and annealing model. *Geochim. Cosmochim. Acta* **73**, 2347–2365 (2009).
82. J. E. Johnson, R. M. Flowers, G. B. Baird, K. H. Mahan, "Inverted" zircon and apatite (U–Th)/He dates from the front range, Colorado: High-damage zircon as a low-temperature (< 50° C) thermochronometer. *Earth Planet. Sci. Lett.* **466**, 80–90 (2017).
83. J. Powell, D. Schneider, D. Stockli, K. Fallas, Zircon (U-Th)/He thermochronology of Neoproterozoic strata from the Mackenzie Mountains, Canada: Implications for the Phanerozoic exhumation and deformation history of the northern Canadian Cordillera. *Tectonics* **35**, 663–689 (2016).
84. U. Ginster, P. W. Reiners, L. Nasdala, Annealing kinetics of radiation damage in zircon. *Geochim. Cosmochim. Acta* **249**, 225–246 (2019).
85. A. K. Ault, W. R. Guenthner, A. C. Moser, G. H. Miller, K. A. Refsnider, Zircon grain selection reveals (de) coupled metamictization, radiation damage, and He diffusivity. *Chem. Geol.* **490**, 1–12 (2018).
86. R. A. Ketcham, C. Gautheron, L. Tassan-Got, Accounting for long alpha-particle stopping distances in (U–Th–Sm)/He geochronology: Refinement of the baseline case. *Geochim. Cosmochim. Acta* **75**, 7779–7791 (2011).
87. D. I. Benn *et al*., Orbitally forced ice sheet fluctuations during the Marinoan Snowball Earth glaciation. *Nat. Geosci.* **8**, 704–707 (2015).
88. A. E. Eyster *et al*., Paleomagnetic evidence for a large rotation of the Yukon block relative to Laurentia: Implications for a low-latitude Sturtian glaciation and the breakup of Rodinia. *Geol. Soc. Am. Bull.* **129**, 38–58 (2017).
89. R. A. Ketcham, R. A. Donelick, M. L. Balestrieri, M. Zattin, Reproducibility of apatite fission-track length data and thermal history reconstruction. *Earth Planet. Sci. Lett.* **284**, 504–515 (2009).